

Article

Carbon Capture from Post-Combustion Flue Gas Using a State-Of-The-Art, Anti-Sublimation, Solid–Vapor Separation Unit

Hani Ababneh , Ahmed AlNouss and Shaheen A. Al-Muhtaseb * 

Department of Chemical Engineering, College of Engineering, Qatar University, Doha P.O. Box 2713, Qatar

* Correspondence: s.almuhtaseb@qu.edu.qa

Abstract: This work attempts to address the quest of removing carbon dioxide from flue gas streams to help preserve the environment. It is based on a model that is able to describe the solid-liquid-vapour and solid-vapour phase equilibria for the ternary system of N_2 - O_2 - CO_2 at pressures from 5 to 130 bar and over a wide range of temperature (140 to 220 K). Furthermore, a corresponding state-of-the-art solid-vapor (SV) CO_2 capture/separation unit is developed and introduced in this work. The SV unit was modeled using the Aspen Custom Modeler software by implementing the thermodynamic model developed before. It was then simulated using the Aspen Plus simulator; its performance was studied and analyzed. Moreover, the performance of the unit was optimized and compared to the most conventional corresponding technology used by the industry (i.e., amine-scrubbing). Results proved that for the same output clean gas composition, which contains only 0.3% CO_2 , the developed state-of-the-art SV unit consumes almost half of the energy required by the conventional process. Other advantages of the novel SV separation unit include the lower requirement of capital equipment, no need of additional agents (such as solvents) and the avoidance of product contamination with such additional agents.



Citation: Ababneh, H.; AlNouss, A.; Al-Muhtaseb, S.A. Carbon Capture from Post-Combustion Flue Gas Using a State-Of-The-Art, Anti-Sublimation, Solid–Vapor Separation Unit. *Processes* **2022**, *10*, 2406. <https://doi.org/10.3390/pr10112406>

Academic Editors: Javier Fernandez Garcia and Enrico Andreoli

Received: 1 September 2022

Accepted: 15 September 2022

Published: 15 November 2022

Publisher's Note: MDPI stays neutral with regard to jurisdictional claims in published maps and institutional affiliations.



Copyright: © 2022 by the authors. Licensee MDPI, Basel, Switzerland. This article is an open access article distributed under the terms and conditions of the Creative Commons Attribution (CC BY) license (<https://creativecommons.org/licenses/by/4.0/>).

Keywords: carbon capture; cryogenic CO_2 separation; solid phase formation; solid–liquid–vapor equilibrium; freezing prediction

1. Introduction

Flue gases resulting from the combustion of fossil fuels are among the major sources of carbon dioxide (CO_2) and other greenhouse gases emitted into the atmosphere [1]. Flue gases are mixtures of water vapor (H_2O), nitrogen (N_2), particulates, heavy metals, and acid gases (such as CO_2 and H_2S). Additionally, in the case of incomplete combustion, flue gases contain carbon monoxide (CO) and volatile organic compounds (VOCs) [2]. The typical composition of flue gases emitted from natural gas-fired power plants is 8–10% CO_2 , 18–20% H_2O , 2–3% O_2 , and 67–72% N_2 [3].

Generally, there are three main techniques for carbon capture: post-combustion, oxy-combustion, and pre-combustion [4]. Figure 1 illustrates the three approaches toward carbon capture in energy industry [5]. In the pre-combustion approach, a fossil fuel is converted to syngas (a mixture of H_2 and CO gases) by the means of gasification or reforming processes [6]. Advantages of pre-combustion include the high concentration of CO_2 , hence the process equipment can be smaller and different solvents may be used; which makes the process less energy intensive compared to post-combustion techniques [7]. However, it requires high capital costs for the fossil-fuel-conversion equipment [8]. In the oxy-fuel combustion process, fuel is combusted in a pure oxygen environment instead of using atmospheric air, therefore the resulted flue gas would have higher CO_2 concentrations since there is no nitrogen to dilute it [9]. On one hand, this technology significantly reduces the cost and the energy needed for carbon capture. On the other hand, the need for an air separation unit needed to produce an oxygen-rich atmosphere sharply increases the overall capital cost [6].

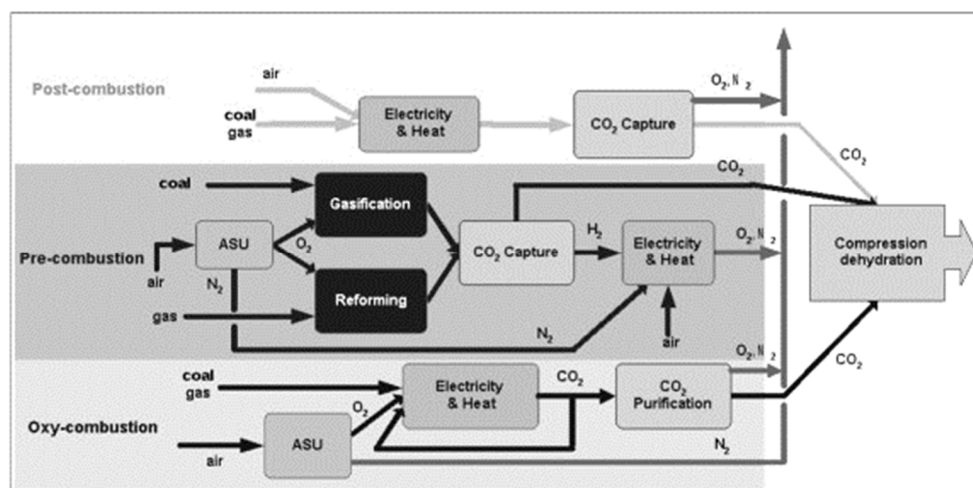


Figure 1. The three main approaches for CO₂ capture [5].

In the post-combustion approach, CO₂ is sequestered from the flue gas stream after the complete combustion of fuels [10]. Post-combustion technologies can be easily integrated with most existing fossil-fuel operated plants. However, the main drawback of this approach is the relatively low CO₂ concentration in the flue gas, which increases the separation difficulty [4]. There are many post-combustion carbon capture technologies such as [11], sorbents [12–14], membrane-separation [15] and solvent-based absorption [16]. The most widely used post-combustion carbon capture technology in the industry is the solvent (e.g., amine)-based absorption technology. Nonetheless, this technology suffers from the high-energy requirements to regenerate and reuse the required solvent and the high maintenance and operation costs [17]. The cryogenic separation technologies have caught the attention of engineers and scientists as a new alternative technology to capture CO₂ from flue gas mixtures. The cryogenic separation offers few advantages over the solvent-based absorption technology; including the lower environmental footprint, eliminating the need for solvents (which eliminates the possibilities of product contaminations) and the lower cost to build and operate [18]. The cryogenic separation is a physical process, which relies on the differences in volatility between CO₂ and the other gases in flue gas to separate the carbon dioxide in a different phase at very low temperatures [5]. The cryogenic separation techniques could be divided into conventional methods (e.g., liquid–vapor separation), nonconventional methods (e.g., solid–vapor separation) [19], and hybrid methods [20]. Depending on the technology utilized, the solid formation could be desirable or avoidable. For example, the Controlled Freezing Zone (CFZ)TM technology depends on the solid formation to improve the separation process [21]. Therefore, it is important to determine accurately the corresponding phase envelopes and the thermodynamic phase equilibrium data to model, design and size the units and equipment of cryogenic separation processes. The thermodynamic equilibrium data needed include vapor–liquid equilibrium (VLE), solid–liquid equilibrium (SLE), solid–vapor equilibrium (SVE), and solid–liquid–vapor equilibrium (SLVE).

The equilibrium data involving a solid phase for the binary system N₂–CO₂ are few and limited. The SVE of this binary system was studied experimentally by Sonntag and Van Wilen [22] and Smith et al. [23], while SLE studies included those of Rest et al. [24], Yaki-menko et al. [25], and Fedorova [26]. SLVE experiments were conducted by Schweitzer [27] and Fandino et al. [28]. To the best of our knowledge, no published SVE or SLVE experimental data are available for the binary system O₂–CO₂; whereas the only available equilibrium data that involves a solid phase is SLE data [24,26,29,30]. On the other hand, no solid formation is anticipated within practical operating conditions for the binary system O₂–N₂. Thus, only VLE data of this system are considered.

A recent study by De Guido and Pellegrini [31] has attempted to predict the SVE for flue gas mixtures using an approach based on the Peng Robinson equation of state [32]. Their proposed model was validated for the SVE data for the binary system N_2 - CO_2 , and was later utilized to predict the SVE for the ternary system N_2 - O_2 - CO_2 . While the model proved successful, the study has not discussed SLVE for the systems, and it only considered one mixture of the ternary system (14.0% CO_2 , 83.0% N_2 and 3.0% O_2 by mole). In a different study by Baxter et al. [33], a cryogenic CO_2 capture (CCC) process from flue gas was proposed by reaching the CO_2 anti-sublimation temperatures (-100 to -135 °C), hence converting CO_2 from the vapor phase into a solid phase. The process proved effective (with CO_2 recovery levels reaching 99%) while being energy-efficient. However, this study has not dealt with the SLVE nor attempted to construct the phase envelope for the ternary mixture N_2 - O_2 - CO_2 . Moreover, it only reported the results of one composition of this ternary mixture. Maqsood et al. [34] developed a hybrid cryogenic network for separating CO_2 from a CH_4 - CO_2 mixture. The network consists of a packed bed and a cryogenic separator. The study was conducted in the phase regions of vapor–solid (VS) (in a packed bed), vapor–liquid (VL) (in a cryogenic separator) and vapor–liquid–solid (VLS) (in a combination of the two units). Their results indicated that energy consumption in the packed bed- cryogenic separator combined unit was about 37% of the energy required by the conventional cryogenic distillation network. However, their study dealt only with the CH_4 - CO_2 binary mixture; and was not expanded to include the binary mixture of CH_4 - H_2S nor the ternary mixture of CH_4 - CO_2 - H_2S . Furthermore, the results were not compared to the industry-common amine sweetening process. Tuinier et al. [35] have developed a cyclic process to capture CO_2 from flue using cryogenically cooled packed beds. However, in their study, the flue gas mixture consists of H_2O , N_2 , and O_2 ; but have not studied the impact of oxygen in the flue in the mixture. They estimated that cooling duty to recover >99% CO_2 from a flue gas (10% CO_2 , 1% H_2O , and 89% N_2) is 1.8 MJ/kg CO_2 . They further developed their process in a different study [36], and used cryogenic packed beds to capture CO_2 from biogas stream. Their study [36] focused on the CH_4/CO_2 ; and their results indicated that the energy duty (to recover one kg of methane from a feed consisting of 45 vol % CO_2 and 55 vol % CH_4) is 2.9 MJ. Unfortunately, these studies do not discuss the liquid and solid formation during the process, nor cover the thermodynamic sides of the process.

This study contributes to the field by two important points. The first important contribution is developing an empirical correlation model based on the Peng–Robinson equation of state (PR EoS), with fugacity expressions, that is able to describe the SLVE and SVE behaviors for the ternary system of N_2 - O_2 - CO_2 at wide ranges of pressures and temperatures. The model predictions will be compared to the experimental data available in the literature to confirm its accuracy and reliability. While the second important contribution of this study is that; for the first time; a carbon capture separation unit from flue gas is modeled and simulated based on the thermodynamic models suggested in this study. The carbon capture unit would operate in the SVE region to separate CO_2 by anti-sublimation. Ultimately, this study aims to compare the performance and energy consumption of this state-of-the-art SV separation unit with the traditional amine-based CO_2 capture unit. The importance of this study is that it will provide researchers and the industry with a novel tool to predict the ternary solid-fluid phase equilibrium behavior of flue gases (represented by N_2 - O_2 - CO_2) as well as the separation of carbon dioxide from this mixture without the need for experimental data, thus saving cost and time. Additionally, it lays the basis for the development of SV separation for CO_2 capture from flue gases.

2. Methodology

The first stage of this study was to develop a suitable mathematical model to predict and describe the SVE, SLE and SLVE behaviors for binary and ternary system of N_2 , O_2 and CO_2 . Following that, the model was optimized by fitting its interaction parameter to provide the best match of the experimental data of the corresponding binary systems available in the literature. Then, the model was used with the optimized interaction pa-

parameters to predict the corresponding equilibrium data and simulate an SV separation unit that is able to capture CO₂ from flue gas stream and collect it in liquid phase. The modelling work was completed using the Aspen Custom Modeler® (ACM) software, which is a process and equipment model development and simulation tool that is compatible with the simulation software packages of Aspen Plus and Aspen Hysys. The ACM has built-in codes, which are specific to chemical engineering applications involving thermodynamic properties such as fugacity and activity coefficients. The ACM has access to Aspen components and properties databases, which makes the software suitable for various chemical engineering applications.

While there are many approaches to model and describe the SLVE behavior [37–39], Ababneh and Al-Muhtaseb have successfully developed an empirical model based on the Peng-Robinson equation of state (PR EoS) to model the SLVE for the binary and ternary systems of CH₄-CO₂-H₂S [17] and N₂-Kr-Xe [40]. The same model will be applied to the system of consideration in this study. This model aims to provide a good description of the SVE and SLVE region of systems involving binary and ternary mixtures involving CO₂, N₂ and O₂. The details of the model are described in the following sections.

2.1. The Proposed Model

At the phase equilibrium of mixtures, the chemical potential of each component in each coexisting phase has to be equal. For example, at the SLVE, the chemical potential equation will be

$$\mu_i^S(T, P) = \mu_i^F(T, P, x^F) \quad (1)$$

where μ_i^S and μ_i^F are the chemical potentials of the component i in a solid phase (which typically consists of a single component—such as CO₂) and in the coexisting fluid (vapor or liquid) phase, respectively; at the system's temperature (T), pressure (P); and the molar composition of component i in the fluid phase (x^F). In the case of the reference state being the ideal gas, Equation (1) can be dealt with in terms of fugacities as [41]:

$$f_i^S(T, P) = f_i^F(T, P, x^F) \quad (2)$$

The solid phase and fluid phase fugacities of component i (f_i^S and f_i^F , respectively) can be calculated from [42]

$$f_i^S(T, P) = \hat{\varphi}_{0i}^{Sat}(T, P_i^{Sub}) P_{0i}^{Sat}(T) \exp\left[\frac{v_{0i}^s}{RT}(P - P_{0i}^{Sat}(T))\right] \quad (3)$$

$$f_i^F(T, P, x^F) = x_i^F \hat{\varphi}_i^F(T, P, x^F) P \quad (4)$$

where $P_{0i}^{Sat}(T)$ is the saturation (sublimation) pressure of the solid-forming component at T , and $\hat{\varphi}_{0i}^{Sat}(T, P_i^{Sub})$ is the fugacity coefficient of the solid component at T and P_{0i}^{Sat} . Furthermore, $\hat{\varphi}_i^F(T, P, x^F)$ is the fugacity coefficient of the component i in the fluid (vapor or liquid) mixture (of molar composition x^F at T and P), and v_{0i}^s is solid molar volume of the component i at the given conditions.

To calculate the fugacity terms of the liquid and vapour phases in Equations (2)–(4), a suitable equation of state (EoS) is used. Furthermore, the sublimation pressure of the solid-forming component at the given temperature has to be found. In this study, it is assumed that the solid phase is incompressible, and the Peng-Robinson equation of state (PR EoS) [32] is used to estimate the fugacity coefficients in the fluid phases ($\hat{\varphi}_i^V$ and $\hat{\varphi}_i^L$) as described in our previous study [17]. The details of PR EoS and the corresponding fugacity expressions can be found elsewhere [32].

2.2. SLVE Modelling of the Binary System N₂-CO₂

At the SLVE for the binary system N₂-CO₂, the solid phase will consist of pure CO₂. Therefore, the equilibrium equations for CO₂ are represented in Equations (5) and (6), and that for N₂ is found in Equation (7).

$$\hat{f}_{\text{CO}_2}^{\text{V}} = \hat{f}_{\text{CO}_2}^{\text{L}} \quad (5)$$

$$\hat{f}_{\text{CO}_2}^{\text{V}} = \hat{f}_{\text{CO}_2}^{\text{S}} \quad (6)$$

$$\hat{f}_{\text{N}_2}^{\text{V}} = \hat{f}_{\text{N}_2}^{\text{L}} \quad (7)$$

The fugacity terms $\hat{f}_{\text{CO}_2}^{\text{V}}$, $\hat{f}_{\text{CO}_2}^{\text{L}}$, $\hat{f}_{\text{N}_2}^{\text{V}}$ and $\hat{f}_{\text{N}_2}^{\text{L}}$ could be found using Equations (8)–(11).

$$\hat{f}_{\text{CO}_2}^{\text{V}} = y_{\text{CO}_2} \hat{\varphi}_{\text{CO}_2}^{\text{V}} P \quad (8)$$

$$\hat{f}_{\text{CO}_2}^{\text{L}} = x_{\text{CO}_2} \hat{\varphi}_{\text{CO}_2}^{\text{L}} P \quad (9)$$

$$\hat{f}_{\text{N}_2}^{\text{V}} = y_{\text{N}_2} \hat{\varphi}_{\text{N}_2}^{\text{V}} P \quad (10)$$

$$\hat{f}_{\text{N}_2}^{\text{L}} = x_{\text{N}_2} \hat{\varphi}_{\text{N}_2}^{\text{L}} P \quad (11)$$

On the other hand, the solid phase fugacity for CO₂ is found from

$$\hat{f}_{\text{CO}_2}^{\text{S}} = x_{\text{CO}_2} \hat{\varphi}_{\text{CO}_2}^{\text{Sub}} \left(T, P_{\text{CO}_2}^{\text{Sub}} \right) P_{\text{CO}_2}^{\text{Sub}} \exp \left[\frac{v_{\text{CO}_2}^{\text{S}}}{RT} (P - P_{\text{CO}_2}^{\text{Sub}}) \right] \quad (12)$$

The sublimation pressure $P_{\text{CO}_2}^{\text{Sub}}$ can be calculated in terms of temperature (T) from

$$\ln \left(\frac{P_{\text{CO}_2}^{\text{Sub}}}{P_t} \right) = \frac{T_t}{T} \left[-14.740846 \left(1 - \frac{T}{T_t} \right) + 2.4327015 \left(1 - \frac{T}{T_t} \right)^{1.9} \pm 5.3061778 \left(1 - \frac{T}{T_t} \right)^{2.9} \right] \quad (13)$$

where ($T_t = 216.592$ K, $P_t = 0.51795$ MPa) are the triple point conditions of pure CO₂.

2.3. SLVE Modelling of the Binary System O₂-CO₂

Similar to the binary system N₂-CO₂, the solid phase at the SLVE of the binary system O₂-CO₂ consists of pure carbon dioxide. Therefore, the phase equilibrium equations for CO₂ are described by Equations (5) and (6); whereas that for O₂ is given by

$$\hat{f}_{\text{O}_2}^{\text{V}} = \hat{f}_{\text{O}_2}^{\text{L}} \quad (14)$$

The fugacities of CO₂ can be estimated using Equations (8),(9) and (12), whereas those of O₂ are estimated from

$$\hat{f}_{\text{O}_2}^{\text{V}} = y_{\text{O}_2} \hat{\varphi}_{\text{O}_2}^{\text{V}} P \quad (15)$$

$$\hat{f}_{\text{O}_2}^{\text{L}} = x_{\text{O}_2} \hat{\varphi}_{\text{O}_2}^{\text{L}} P \quad (16)$$

2.4. SLVE Modelling of the Binary System N₂-O₂

For the binary system N₂-O₂, no solid phase is present within the studied range of temperature. Therefore, only the vapour and liquid phases are present; and hence no

need to optimize the model for the SVE or SLVE of this system. The PR EoS is capable of describing the vapour-liquid equilibria (VLE) of this system; and is already optimized with the interaction parameter k_{ij} value of -0.0119 [43].

2.5. SLVE Modelling of the Ternary System N_2 - O_2 - CO_2

As per the degrees of freedom rule [44] when three components and three coexisting phases are present, the degree of freedom would be 2. Therefore, to study the SLVE locus for the ternary system N_2 - O_2 - CO_2 , an equilibrium stage separation unit was modeled and used to construct the SLVE locus for three different mixtures of the ternary system (i.e., the solid, liquid and vapor phase mixtures). The temperature and pressure of the equilibrium stage separation unit are to be determined in order to determine the state of the corresponding system. The feed stream to the unit is separated at a certain temperature and pressure into either three phases (vapor, liquid and solid) or two phases (vapor and solid) depending on the corresponding conditions. In each case, the solid phase is assumed to consist of pure CO_2 .

The system is modeled as an equilibrium stage separation unit, while assuming that the feed stream (F) consists of the feed compositions (Z_i). The material balance equations used for the first case (SLVE) are:

Total Material Balance:

$$F = V + L + S_{CO_2} \quad (17)$$

Material Balance on CO_2 :

$$Z_{CO_2}F = y_{CO_2}V + x_{CO_2}L + S_{CO_2} \quad (18)$$

Material Balance on N_2 :

$$Z_{N_2}F = y_{N_2}V + x_{N_2}L \quad (19)$$

The corresponding phase equilibrium equations for CO_2 are given in Equations (5) and (6), that for N_2 is given in Equation (7); and that for O_2 is given in Equation (14). Additionally, the fugacity terms can be obtained from Equations (8), (9) and (12) for CO_2 , from Equations (10) and (11) for N_2 and from Equations (15) and (16) for O_2 .

For the second case (VSE), the vapour phase will be present with the absence of liquid phase; the corresponding material balance equations are:

Total Material Balance:

$$F = V + S_{CO_2} \quad (20)$$

Material Balance on CO_2 :

$$Z_{CO_2}F = y_{CO_2}V + S_{CO_2} \quad (21)$$

Material Balance on N_2 :

$$Z_{N_2}F = y_{N_2}V \quad (22)$$

The corresponding equilibrium equations for CO_2 is given by Equation (6). Furthermore, the fugacity values of CO_2 in vapour and solid phases can be obtained from Equations (8) and (12), respectively; and those of N_2 and O_2 in the vapour phase can be obtained from Equations (10) and (15), respectively.

2.6. Modelling of the Solid-Vapour (SV) Separation Unit

Figure 2 shows a schematic diagram of the SV separation unit. The separation unit consists of a solid-vapor equilibrium (SVE) separation zone and a heated melting tray underneath the equilibrium zone to melt the solid phase to be collected as a liquid.

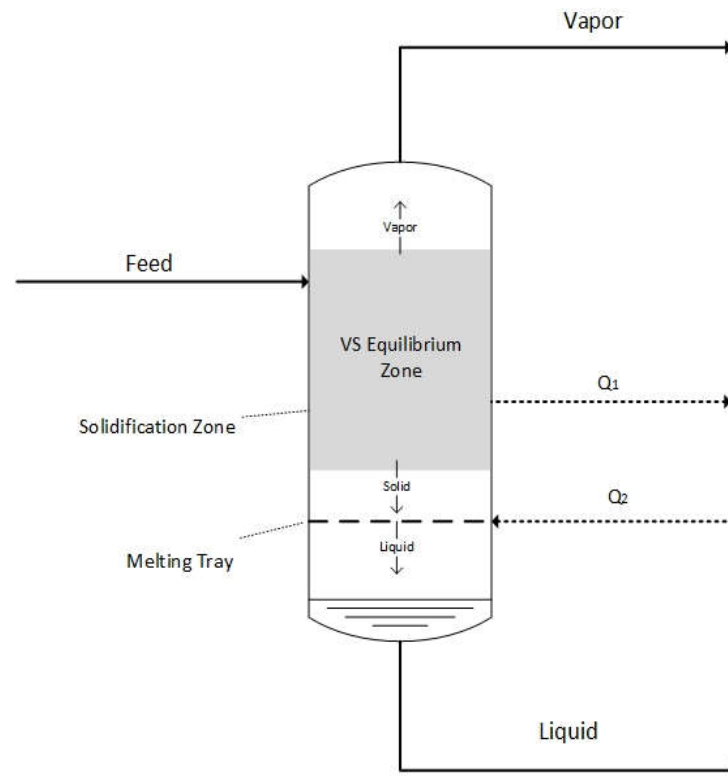


Figure 2. Schematic diagram for the suggested SV separation unit.

The feed stream enters the unit at its operating pressure and at a low temperature (in the range of 200–230 K), so it will be close the solidification temperature, which is usually from 200–215 K. In the SVE zone (where only CO₂ solidifies; and nitrogen, oxygen and traces of CO₂ remain in the vapor phase). The temperature is further dropped by cooling (with a cooling rate of \dot{Q}_1) to ensure that the unit is operating in the SVE zone. The solid CO₂ would descend down due to its higher density, reaching the melting tray, at which a heating rate (\dot{Q}_2) is supplied to melt the solid CO₂ into a liquid stream. The formed liquid stream can be collected at the bottom of the unit, while the top vapor stream will consist mostly of N₂ and O₂. A similar unit was successfully simulated in our previous study for natural gas sweetening [45], and it showed excellent energy savings when compared to industry-common gas sweetening units.

In the SVE solidification zone, the equilibrium equations were discussed in the previous section. Furthermore, the material balance equations for the SV separation unit are given by

Total Material Balance:

$$\dot{n}_{Feed} = \dot{n}_{Vapor} + \dot{n}_{Liquid} \quad (23)$$

Material Balance on N₂:

$$z_{N_2} \dot{n}_{Feed} = y_{N_2} \dot{n}_{Vapor} \quad (24)$$

Material Balance on CO₂:

$$z_{CO_2} \dot{n}_{Feed} = y_{CO_2} \dot{n}_{Vapor} + x_{CO_2} \dot{n}_{Liquid} \quad (25)$$

where

$$\dot{n}_{Liquid} = \dot{n}_{Solid} = \dot{n}_{Solid-CO_2} \quad (26)$$

$$x_{CO_2} = 1 \quad (27)$$

$$y_{N_2} + y_{CO_2} + y_{O_2} = 1 \quad (28)$$

\dot{n}_{Feed} , \dot{n}_{Vapor} and \dot{n}_{Solid} are the total molar flow rates of the feed stream, vapour stream and solid (or liquid) streams, respectively; and Z_i is the mole fraction of the component i in the feed.

The separation unit has two heat utility streams: \dot{Q}_1 and \dot{Q}_2 . \dot{Q}_1 is for cooling the feed stream to achieve the needed temperature of the SVE zone, whereas \dot{Q}_2 is for heating required to melt the solid CO₂ formed in the SVE zone. Figure 3 better explains the mass and energy flow schemes for the SV separation unit.

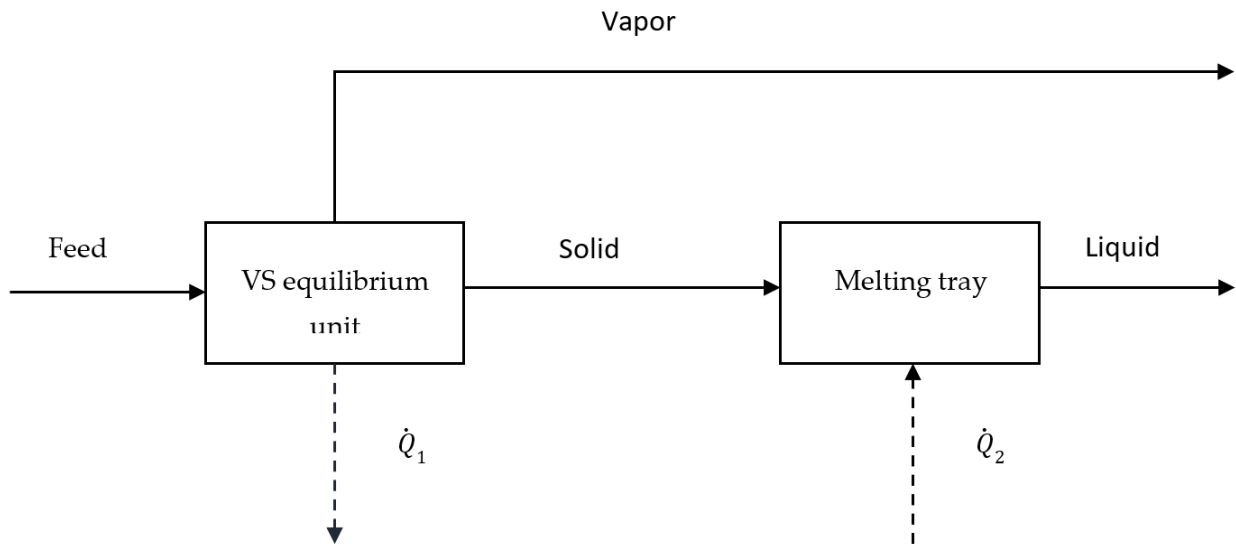


Figure 3. Simplified mass and energy flows for the SV separation unit.

These cooling and heating rates can be estimated from the following steady-state energy balances on the two subsystems illustrated in Figure 3:

$$\dot{Q}_1 = \dot{H}_{Feed} - (\dot{H}_{Vapor} + \dot{H}_{Solids}) \quad (29)$$

$$\dot{Q}_2 = \dot{H}_{Liquid} - \dot{H}_{Solids} \quad (30)$$

where

$$\dot{H}_{Feed} = \dot{n}_{Feed} h_{Liquid}(T_{Feed}, P_{Feed}) \quad (31)$$

$$\dot{H}_{Vapor} = \dot{n}_{Vapor} h_{Vapor}(T, P) \quad (32)$$

$$\dot{H}_{Liquid} = \dot{n}_{Liquid} h_{Liquid}(T, P) \quad (33)$$

and

$$\dot{H}_{Solids} = \dot{n}_{Solid_CO_2} h_{Solid_CO_2} \quad (34)$$

where \dot{H} is the enthalpy flow rate, h is the molar enthalpy of the component/stream. Specifically, h_{Vapor} is the molar enthalpy of the vapor stream emerging from the SVE unit; whereas h_{Liquid} and h_{Solid} are, respectively, the molar enthalpies of pure CO₂ in the liquid stream emerging from the melting tray and the solid stream entering to the melting tray at T and P . The enthalpies h_{Vapor} and h_{Liquid} are determined at the corresponding conditions by the built-in Aspen Plus models. Furthermore, the molar enthalpy of the solid phase can be estimated from

$$h_{Solid_CO_2}(T, P) = h_{Vapor_CO_2}(T, P) - \Delta h_{CO_2}^{sub} \quad (35)$$

where $\Delta h_{CO_2}^{sub}$ is the enthalpy of sublimation of CO₂; which equals 28.83 kJ/mol [46].

3. Results and Discussion

3.1. Correlation of the Binary System of N_2 - CO_2

To the authors' knowledge, the data available by Schweitzer [27] and Fandino et al. [28] are the only experimental data available in the literature for SLVE of the N_2 - CO_2 binary system. The data by Fandino et al. [28] is limited and only include only four points, while the data by Schweitzer include 14 points in the range of 12–130 bar. The studies discussing the SVE of the N_2 - CO_2 binary system include those by Sonntag and Wylen [22], and Smith et al. [23]. The latter study covers the pressure range of 51–200 bar, while that of Sonntag and Wylen [22] was conducted in the pressure range between 5 and 101 bar. Both studies reported the mole fraction of CO_2 in the vapor phase at temperatures between 140 K and 190 K. Due to their convenient ranges of conditions, our model will be optimized based on the SVE dataset by Sonntag and Wylen [22] in addition to the SLVE data by Schweitzer [27]. Therefore the optimized interaction parameter to be obtained would be applicable for both the SLVE locus and SVE regions. To optimize the model, it was first exported into the Aspen Plus simulator, where the Aspen Plus regression tool was used. The target was to better match the model predictions with data by Schweitzer for the SLVE locus [27] and Sonntag and Wylen [22] for the SVE region by manipulating the interaction parameter k_{ij} . The target was to minimize the value of the objective function as built in the Aspen Plus simulator. The objective function equation is described elsewhere [47].

The interaction parameter was varied between -0.1000 and $+0.1000$; and the results showed that the optimum interaction parameter k_{ij} was $+0.0405$. Figure 4 shows the optimum model predictions versus the experimental data for the SLVE pressure-temperature (PT) locus, while Figure 5 is comparing the model predictions for the mole fraction of carbon dioxide in the vapor phase in the SVE region to laboratory data reported by Sonntag and Wylen [22].

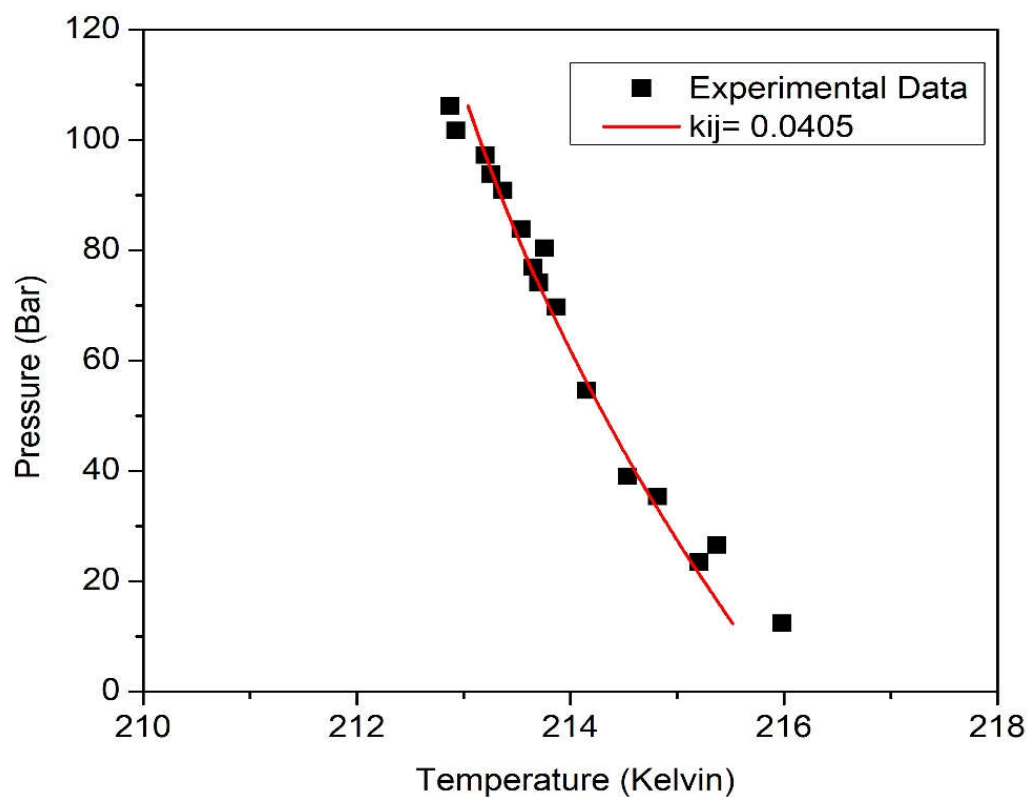


Figure 4. Comparison of model correlation of the SLVE PT locus (line) with the optimum k_{ij} value to the corresponding experimental data (symbols) for the binary system N_2 - CO_2 [22].

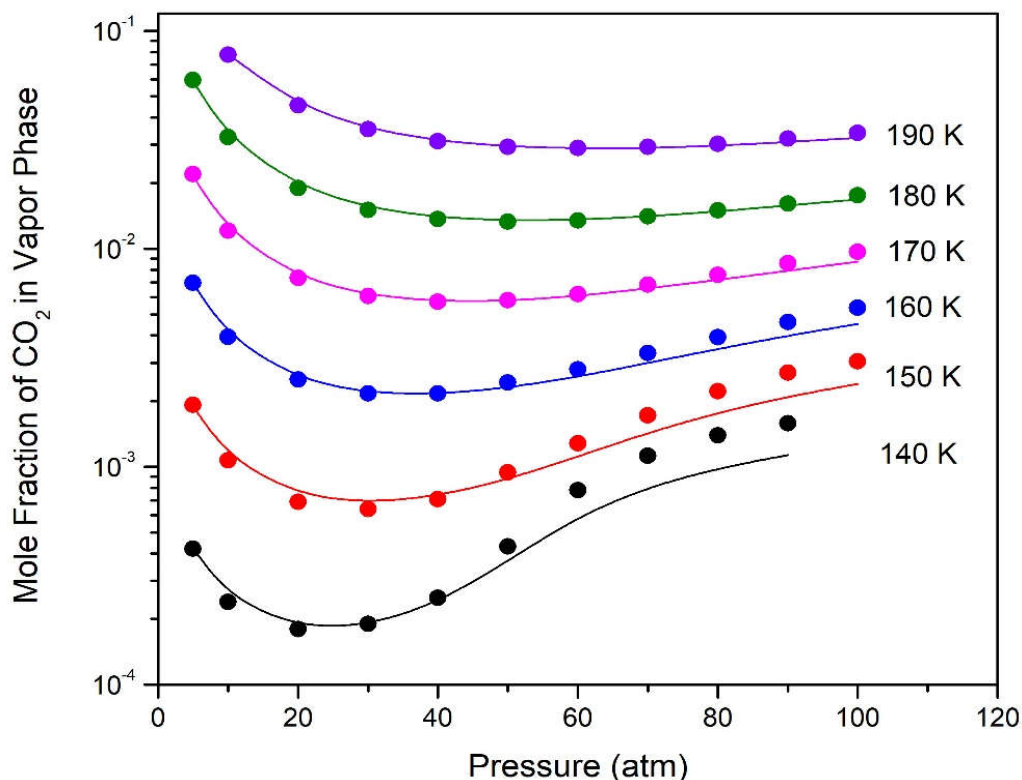


Figure 5. Comparison of model predictions (lines) and experimental data (symbols) [22] of the binary system N_2 - CO_2 for the effect of temperature and pressure on composition of vapor phase in the SVE region.

It could be noticed from Figure 4 that the model has successfully generated the SLVE locus for the binary N_2 - CO_2 binary system, and it was accurate in matching the experimental results as optimized by Aspen Plus. Figure 5 confirms the suitability of the model to represent this binary system in the SVE region; the model predictions for y_{CO_2} was accurate and matched the data reported by Sonntag and Wylen [22], especially at high temperatures (>170 K) or at low temperatures (140–160 K) and low pressures (<50 atm).

3.2. Correlation of the Binary System of O_2 - CO_2

In the absence of experimental SLVE or SVE data for the binary O_2 - CO_2 system, there is no reliable way to optimize the model to better predict this system behavior. However, to the authors' knowledge, only experimental SLE data is available for this binary system [24,29,30]. Riva [48] has regressed these SLE data to find the best value for the interaction parameter. The PR EoS model was used for estimating the fugacities of vapor and liquid phases. Furthermore, the Zabaloy equation was used for the fugacity of the solid phase [49], but the Zabaloy equation was slightly modified as described therein [48]. This approach, which is almost similar to the approach used in this study, has been used model to the CH_4 - CO_2 system, and the optimum value found by Riva et al. [50] was 0.119, which is very close to the corresponding results in our previous study [17], where the optimum interaction parameter value for the same system using the PR EoS was 0.120. Therefore, it is believed to be safe to use the optimum interaction parameter (k_{ij}) found by Riva [48] for the O_2 - CO_2 system, which was 0.160 using the Zabaloy equation, in this study (which uses the PR EoS). Figure 6 shows the SLVE locus predicted by the model described in Section 2.3 using this interaction parameter value ($k_{ij} = 0.160$).

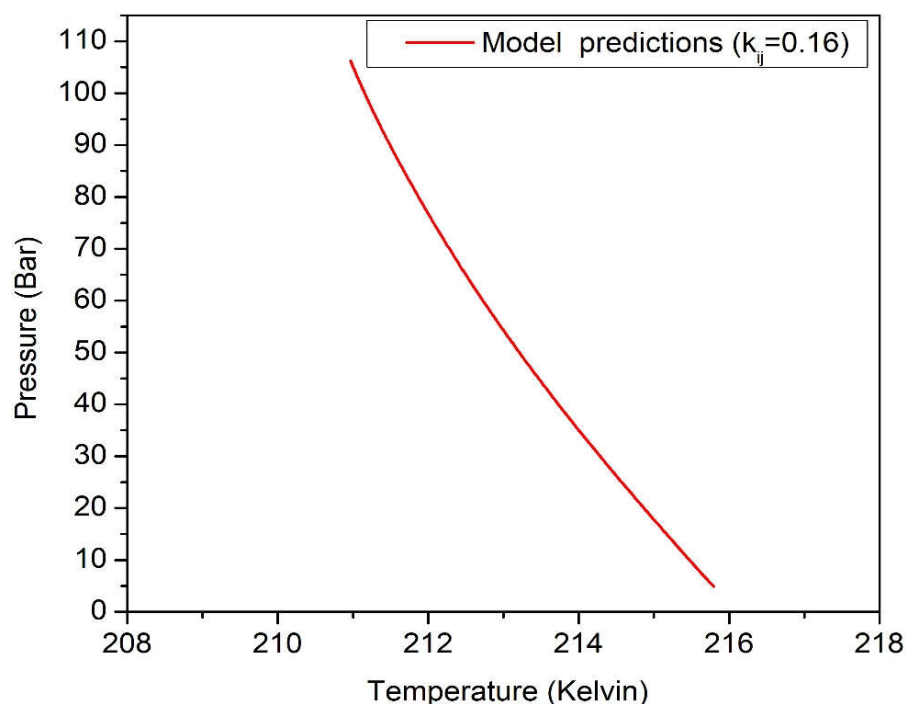


Figure 6. Model predictions for SLVE locus of the binary system O_2 - CO_2 .

3.3. Predictions of the Ternary System N_2 - O_2 - CO_2

To predict the SLVE and the SVE data for this ternary system as described in Section 2.4, the interaction parameters for the constituting binary systems (N_2 - CO_2 , O_2 - CO_2 and N_2 - O_2) are required. As described in the previous sections, the optimum interaction parameters chosen for the N_2 - CO_2 and O_2 - CO_2 binary systems were 0.0405 and 0.160, respectively. Moreover, since the discussed range of temperature in this study (>140 K) is well above the triple point temperatures for N_2 (63.14 K [51]) and O_2 (54.33K [52]), it is not expected to exhibit a solid phase of wither nitrogen or oxygen in the binary system of N_2 - O_2 . Therefore, only the VLE of this system is exhibited, where the corresponding optimum interaction parameter ($k_{ij} = -0.0119$) is used as already found by Sandler [43].

To construct the phase envelope for this ternary system three different feed composition were tested as shown in Table 1. Figure 7 shows the model-predicted phase diagrams for these three cases, where it is clear that the three different mixtures have almost the same SLVE line. However, the point where the SLVE line meets that of the SVE is quite different for different compositions. This meeting point will shift up or down (in pressure and temperature) depending on the ratio of Z_{CO_2}/Z_{N_2} in the mixture. As this ratio increases, the meeting point will move down (lower pressure), moving towards the SVE for pure CO_2 . On the other hand, increasing Z_{O_2} within the mixture would move SLVE line for the ternary system towards the SLVE line for binary system of O_2 - CO_2 . In general having more concentrations of the O_2 and N_2 gases would result in having “smaller” vapor-solid region, therefore in the systems where the CO_2 concentration is low, extra care should be taken in order to ensure operating within the SVE region.

Table 1. Compositions of the feed mixtures utilized to construct the ternary system phase diagrams.

Case	Z_{N_2}	Z_{O_2}	Z_{CO_2}	Z_{CO_2}/Z_{N_2}	Z_{CO_2}/Z_{O_2}	Z_{O_2}/Z_{N_2}
A	0.80	0.05	0.15	0.1875	3.000	0.0625
B	0.75	0.05	0.20	0.2667	4.000	0.0667
C	0.67	0.08	0.25	0.3731	3.125	0.1194

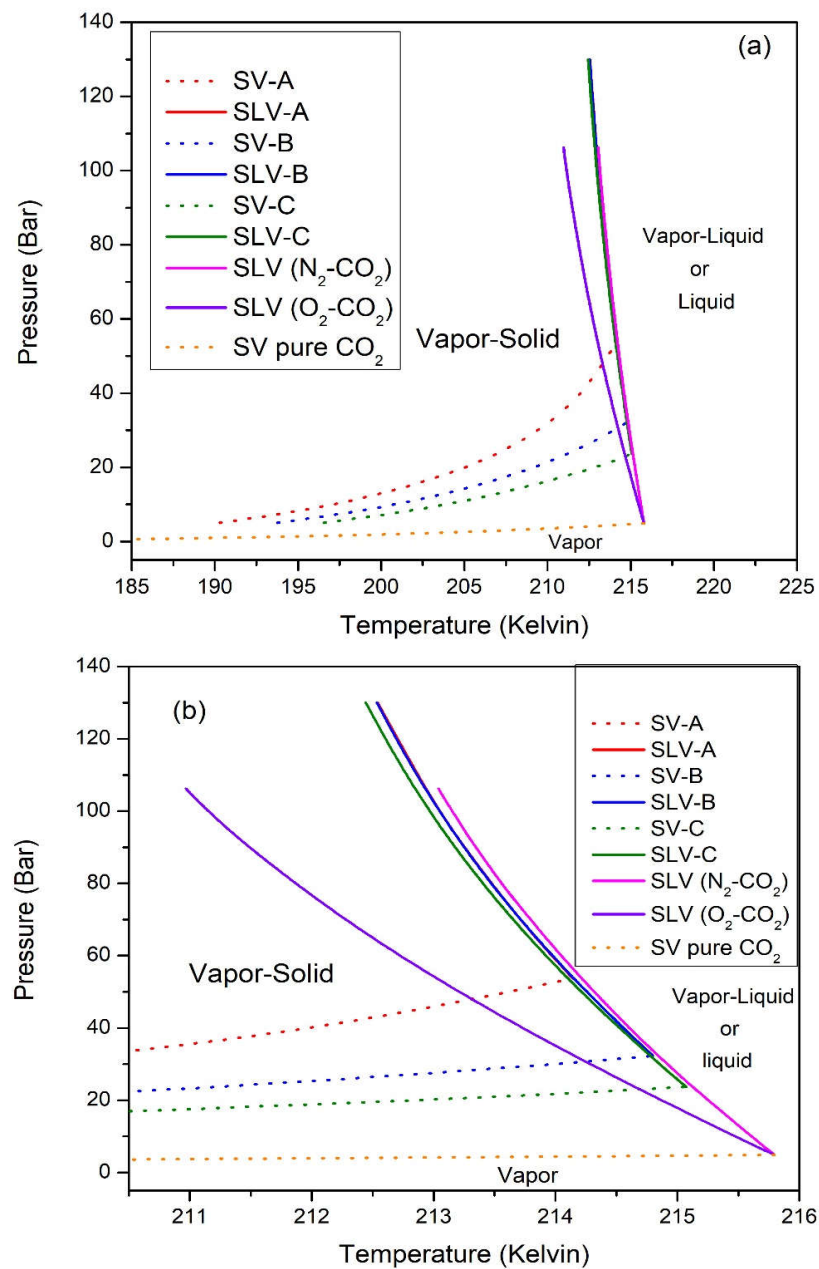


Figure 7. Pressure–temperature phase diagrams for the three cases and compared to SLV locus lines for the binary systems; $\text{N}_2\text{-CO}_2$ and $\text{O}_2\text{-CO}_2$: (a) over the full range of temperatures, and (b) zoomed into the temperature range 210.5–216 K.

The results of this model were compared and validated against those obtained by De Guido and Pellegrini [31]. As mentioned in the introduction, the study by De Guido and Pellegrini has developed a model similar to the one adopted in this work to study the ternary system $\text{N}_2\text{-O}_2\text{-CO}_2$; and they studied one mixture of this system (with a molar composition of 83% N_2 , 3% O_2 , and 14% CO_2). They predicted pressure-temperature (PT) locus data for the CO_2 recoveries of 0% (the frost line), 90%, 95%, and 99%; where the CO_2 recovery is defined by the amount of CO_2 separated in the solid phase relative to that in the feed.

The frost line predicted in this work is compared to that predicted by De Guido and Pellegrini in Figure 8a. In this study, it was found that a part of the frost line (at pressures above 65.4 bar) would be an SLVE locus, while at lower pressures it exhibits an SVE locus line. This result is confirmed by the model as well as the experimental results of the binary

system N_2 - CO_2 [27], which is believed to have a similar behavior to this mixture. This is because the composition studied herein has a minimal concentration of oxygen (3%), hence its behavior will not deviate much from that of the binary system N_2 - CO_2 . Figure 8b compares the PT loci data corresponding to various recoveries of CO_2 in the solid phase as predicted by this work (solid line) and by De Guido and Pellegrini (dashed lines). The results prove that both models behave in very similar ways, especially at lower recoveries (90% and 95%). Nonetheless, a noticeable difference between the two models is noticed for the 99% recovery at high pressures. However, in the study of De Guido and Pellegrini, no attempts have been made to optimize the interaction parameters and their interaction parameter values were taken as-is from the Aspen HYSYS[®] V9.0 process simulator. Therefore, we believe that the results of this study are more accurate since the interaction parameters were optimized, and the frost line is a better representative of similar systems.

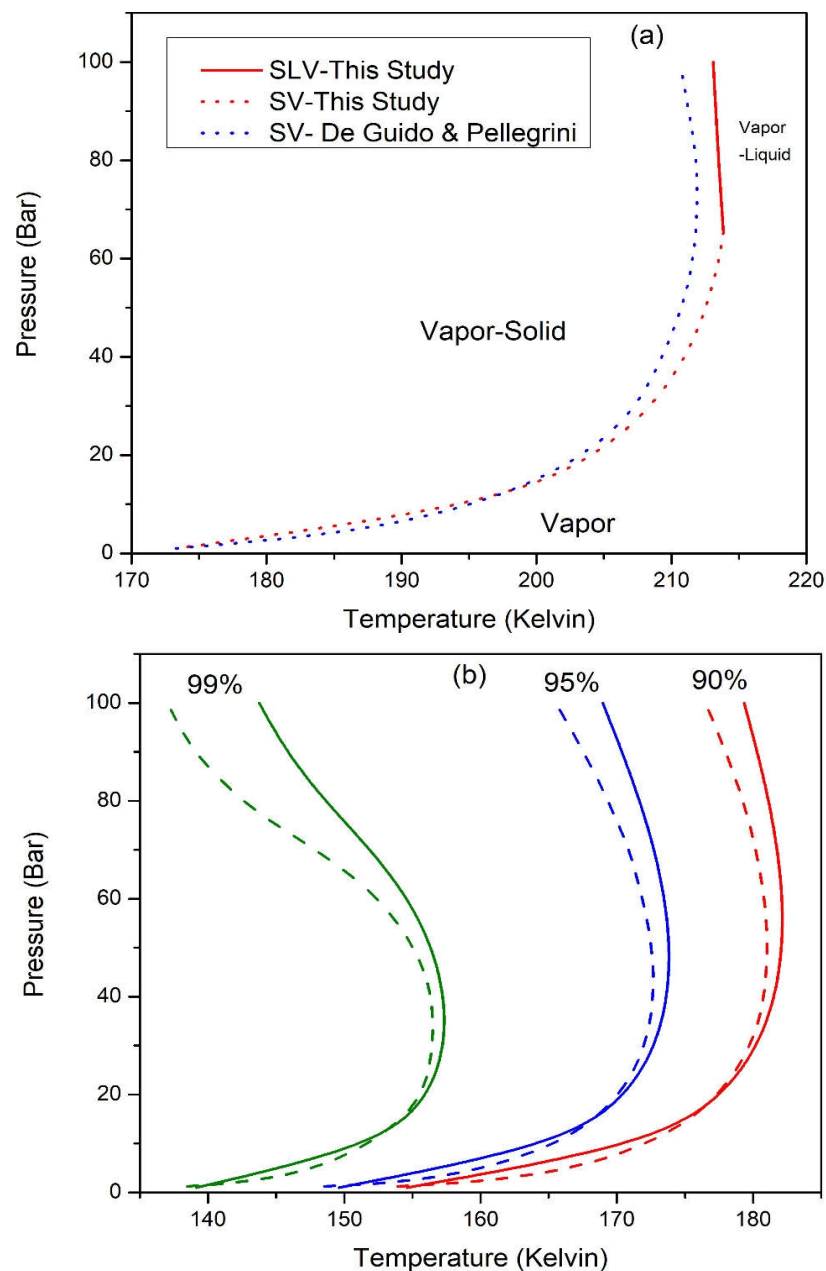


Figure 8. Comparison between results of this study and those of the De Guido and Pellegrini study [24] for the CO_2 recoveries of (a) 0% (frost line) and (b) 90%, 95%, and 99% recovery. Solid and dashed lines represent this study and the study of De Guido and Pellegrini, respectively [31].

3.4. Simulation of SV Separation Unit and Sensitivity Analyses

The SV separation unit model discussed in Section 2.5 was exported from the ACM to Aspen Plus environment for simulation. The following two feed compositions (mole%) were tested:

- Case 1 (86.9% N₂, 11.0% CO₂, 2.1% O₂)
- Case 2 (71.8% N₂, 24.7% CO₂, 3.5% O₂)

These flue gas compositions represent typical dry-basis gas compositions found in the energy industry [3]; where Cases 1 and 2 represent relatively low and high concentrations of CO₂ in the feed, respectively. Table 2 summarizes the feed properties for the two cases.

Table 2. Dry-basis compositions and specifications of the tested flue gas feeds.

Feed		Case 1	Case 2
Dry feed composition	N ₂	86.9%	71.8%
	O ₂	2.1%	3.5%
	CO ₂	11.0%	24.7%
Feed flow rate	kg/h	2986	3210
	kmol/h	100	
Feed conditions	Temperature	280 °C (553.15 K)	
	Pressure	1 atm (1.01325 bar)	

Figure 9 illustrates the process flow diagram of the CO₂ capture process using the SV separation unit. The flue gas feed, which is at 1 atm and 553.15 K was compressed to a pressure between 5 and 50 bar using a compressor. Then, it was cooled down isobarically to a temperature of about 210 °K before entering the SV unit, while the temperature is further dropped (to 140–190 K) to make sure that the unit is operating in SVE region.

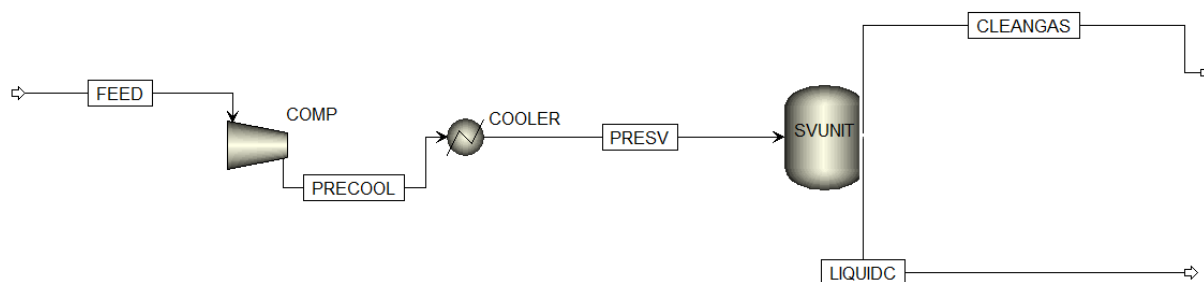


Figure 9. Process flow diagram of the SV CO₂ capture process.

To study the performance of the SV unit, two sensitivity analysis tests were conducted on one of the cases, i.e., “Case 1” presented above in Table 2, as an example to study the effects of the compressor discharge pressure and SV operating temperature on (1) the composition of CO₂ in the effluent output gas stream and (2) the energy requirements for each of the compressor, cooler, and heater; as well as the overall energy consumption.

The first sensitivity analysis studied the effect of compressor discharge pressure (SV unit pressure) and the SV unit’s operating temperature on the composition of the CO₂ in the output clean gas stream. Figure 10 illustrates the results of the first sensitivity analysis tool; where increasing the operating temperature in the SV unit results in increasing the CO₂ composition in clean gas stream emerging from the unit (i.e., reducing CO₂ recovery). Contrary to that is the relationship between the compressor discharge pressure with the mole fraction of CO₂ in the output gas stream; where increasing the discharge pressure decreases the mole fraction of CO₂ in the output gas stream. Nevertheless, the impact of pressure is less significant than that of temperature. For example, increasing the pressure

from 10 to 30 bar would decrease the mole fraction of CO₂ in the output gas stream from 0.004 to 0.0021 (≈50% reduction). However, raising the operating temperature from 160 to 180 K at 30 bar would increase the CO₂ content in the output gas stream by 7 folds.

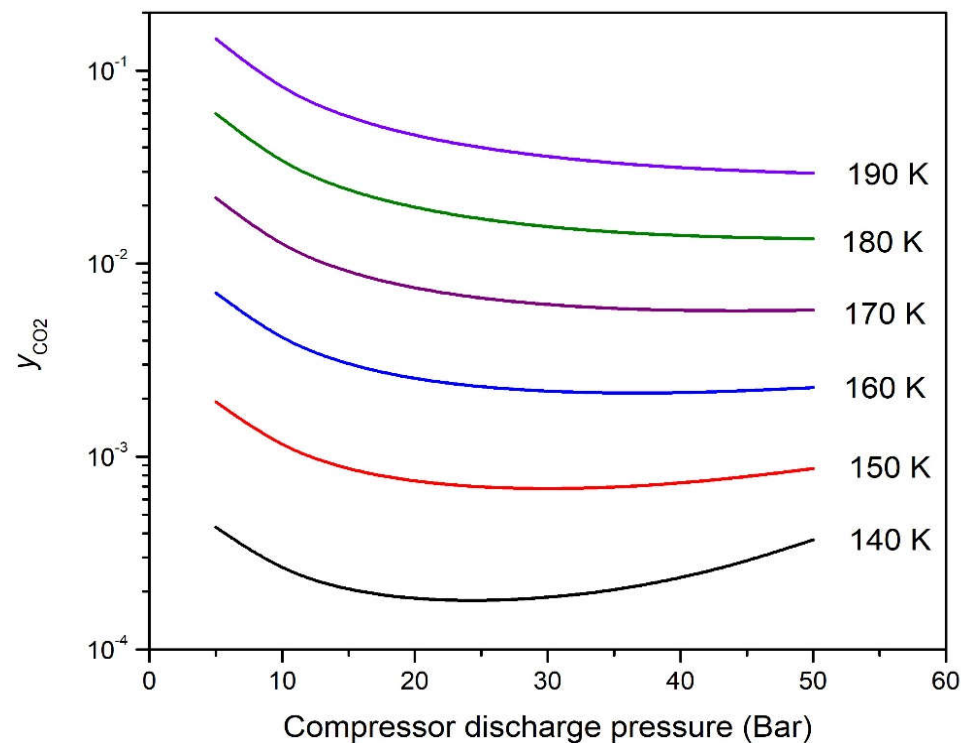


Figure 10. The impact of compressor discharge pressure at different SV operating temperatures on the CO₂ composition in the output clean gas stream.

The second sensitivity analysis test aims to study the impact of the same manipulated variables on compressor power, cooling rate in the cooler, cooling rate in the SV unit (\dot{Q}_1), heating rate needed for melting the solids (\dot{Q}_2), and the overall process energy consumption. The analysis results are shown in Figures 11 and 12. Figure 11a shows the impact of compressor discharge pressure on the energy consumption of the SV separation process, while the unit temperature is fixed at the average value of 160 K. It is clear from the figure that increasing the pressure would increase all of the energy consumption components (cooler cooling rate, compressor work, \dot{Q}_1 and \dot{Q}_2); and as results, it would significantly raise the overall energy requirements. Higher discharge pressures would require more power to compress the flue gas, and more cooling rate in the cooler (since it would raise the temperature of the flue gas exiting from the compressor). However, the discharge pressure has a minimal effect on \dot{Q}_1 and \dot{Q}_2 when the SV temperature is fixed. While both cooling and heating rates (\dot{Q}_1 and \dot{Q}_2) would increase, their change is not significant since the operating temperature of the unit is more influential on its energy requirements as to be observed in Figure 11b. In Figure 11b, the operating temperature was altered while maintaining the compressor discharge pressure at an average value of 30 bars. No change was observed in the energy rates consumed by the compressor or the feed cooler at different SV unit operating temperatures since both of these process components are upstream of the SV unit. However, both of \dot{Q}_1 and \dot{Q}_2 have slightly dropped with the increase of the temperature. The drop of \dot{Q}_1 results from the lower cooling rates needed to achieve higher operating temperature, and that of \dot{Q}_2 results from the less amount of solid CO₂ formed in the unit at higher operating temperature, hence less energy is needed to melt it.

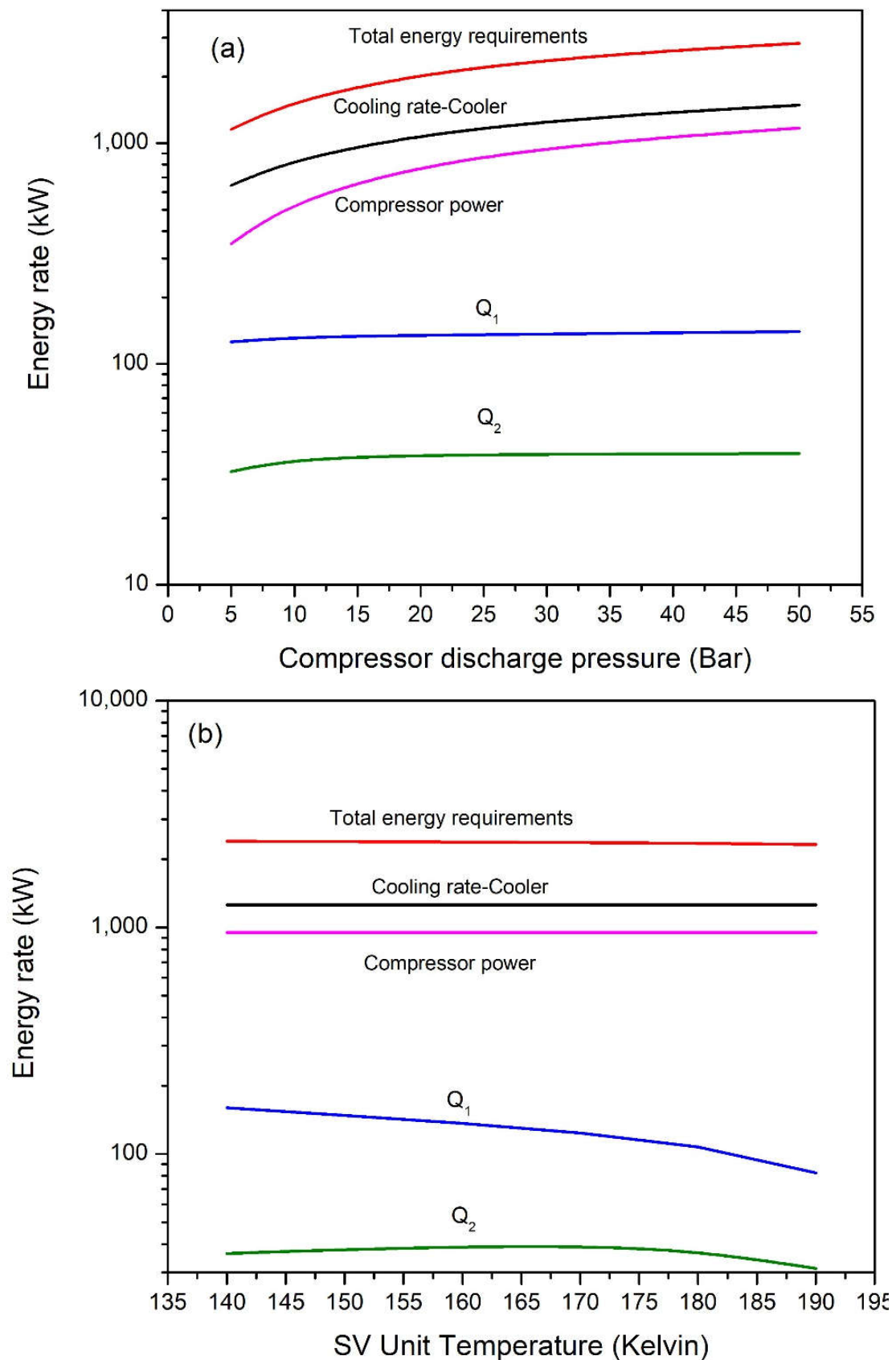


Figure 11. Impact of (a) compressor discharge pressure (at an SV process operating temperature of 160 K) and (b) SV unit operating temperature (at a compressor discharge pressure of 30 bar) on the energy consumption elements of the SV CO₂ capture process.

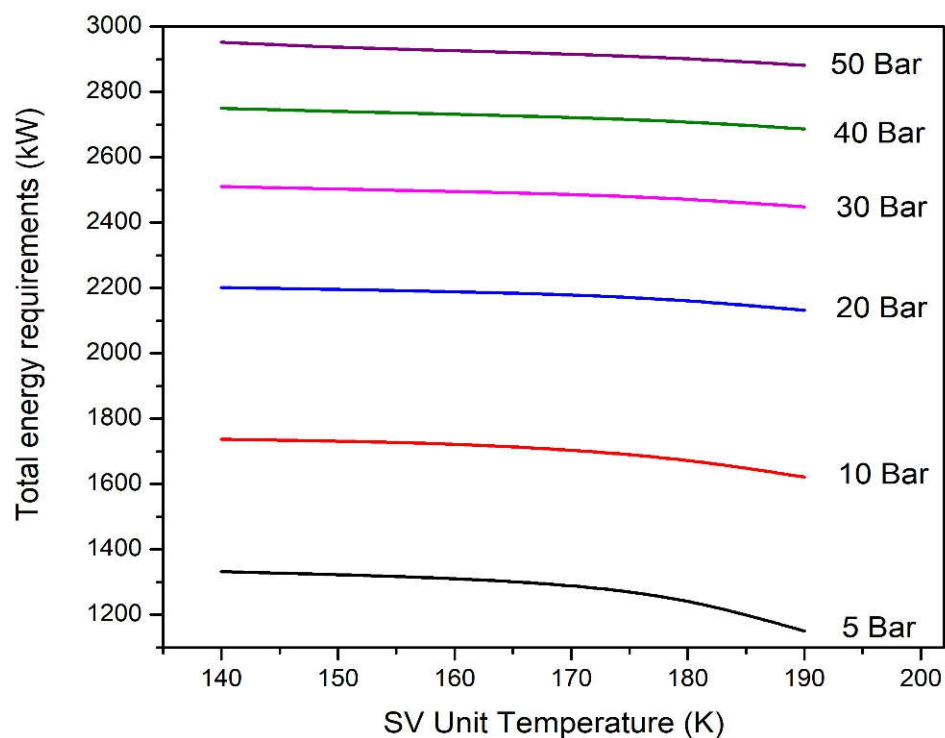


Figure 12. Combined impact of compressor discharge pressure and SV unit operating temperature on the total energy rate consumption of the SV CO₂ capture process.

Figure 12 shows the combined impact of both the compressor's discharge pressure and SV unit operating temperature on the overall energy rate requirements by the process. Overall, the discharge pressure has a more significant impact on the overall energy rate needed for the process when compared to the unit operating temperature. Furthermore, the overall energy requirement decreases by reducing the compressor discharge pressure and/or increasing the SV separation process temperature.

3.5. Comparison with Amine-Based CO₂ Capture Unit

An industry-common amine-based CO₂ capture unit was simulated using the Aspen Hysys® software. Figure 13 shows the process flow diagram of this CO₂ capture process, which consists of a traditional gas-liquid acid gas absorption process at high pressure that uses N-methyldiethanolamine (MDEA) as a chemical solvent to remove CO₂ from the flue gas stream. MDEA is a highly selective solvent that is commonly used to treat sour gases and removes a large proportion of the CO₂ in the feed gas from the system [53]. It is also a key ingredient in many specialty amine formulations designed for deeper CO₂ removal in applications such as synthesis gas production and treating high concentrations of CO₂ in natural gases found in various parts of the world [54]. In recent years, however, attempts have been made to use solvents containing only MDEA for CO₂ removal from high concentration gases, typically at high pressures [54]. In this process, the flue gas is cooled (to a temperature of 311 K) and pressurized (to a pressure of 57 bar) before being fed to the high-pressure absorber, where the CO₂ gas is removed. Acid gases are then stripped from amine by a regenerator column operating at low pressure (1.5 bar) and high temperature (120 °C) using MDEA solvent, which is recycled back to the absorber column with makeup fresh solvent.

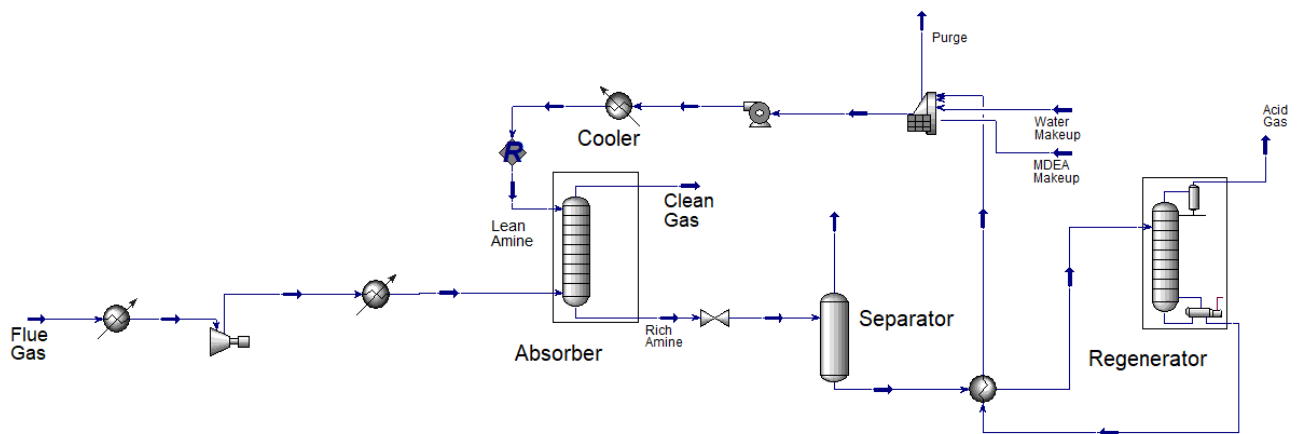


Figure 13. Process flow diagram of the MDEA CO₂ capture process.

The two processes (the novel SV separation process studied in this work and the commercial amine absorption process) were compared to each other on the same basis, using the same feed flow rate, compositions and conditions of the two cases presented in Table 2. The target was to achieve a clean gas output stream with a CO₂ mole fraction that does not exceed 0.3%, while optimizing each process by minimizing the overall energy consumption. The optimized results of the traditional amine CO₂ capture unit and those for the optimized SV separation unit are presented in Tables 3 and 4, respectively.

Table 3. Results for the optimized amine-based CO₂ capture process.

		Case 1	Case 2
Solvent		MDEA	
Solvent flow rate	kg/h	4168.5	9178.2
	kmol/h	143.0	314.5
Output gas composition	N₂	97.1%	94.9%
	O₂	2.4%	4.6%
	CO₂	0.3%	0.3%
	H₂O	0.2%	0.2%
	CO₂ recovery (ratio removed from the feed)	CO₂	97%
Energy requirements (kW)	Flue gas Cooler 1	214.2	226.4
	Flue gas Compressor	680.2	657.8
	Flue gas Cooler 2	687.2	670.1
	Reboiler	259.2	369.4
	Condenser	137.0	109.2
	Pump	8.4	18.6
	Amine cooler	102.0	232.6
	Total	2088.1	2284.1
Output cleangas conditions	Temperature (K)	316.93	
	Pressure (bar)	56.17	

Table 4. Results of the optimized SV separation unit.

		Case 1	Case 2
Output clean gas phase composition (mol%)	N ₂	97.3%	95.1%
	O ₂	2.4%	4.6%
	CO ₂	0.3%	0.3%
CO ₂ recovery (ratio removed from feed)	CO ₂	97%	99.1%
Energy requirements (kW)	Compressor	350.7	345.3
	Cooler	644.1	653.7
	\dot{Q}_1	134.4	245.8
	\dot{Q}_2	33.1	75.3
	Total	1162.1	1320.4
Output clean gas conditions	Temperature (K)	153.4	
	Pressure (bar)	5	

A comparison of the total energy requirements of the two processes shows that the novel SV process developed in this work consumes less energy when compared to the conventional amine-based process. Tables 3 and 4 show that the energy savings by the novel SV separation process ranges between 42% and 44% for Case 2 and Case 1, respectively.

Overall, we may conclude that CO₂ capture using the novel SV separation process offers many benefits compared to conventional amine-based process. The first benefit is the lower energy consumption, hence lower operational costs, than the conventional amine-based process. The second is the elimination of solvent handling equipment, therefore requiring a lower capital cost. This factor would further help avoid contaminating the product gas stream with steam or solvent vapors. Also, lower corrosion rates are anticipated in the units of the novel SV separation process since solvents are no longer required and due to the lower operating temperature.

4. Conclusions

In this study, a state-of-the-art anti-sublimation CO₂ capture unit was developed. This unit is based on its operation in the solid-vapor equilibrium (SVE) region in order to remove CO₂ from flue gas streams by freezing it.

It was noticed that the researchers and scientific community have not studied the thermodynamics of the solid-fluid phase equilibrium behavior for the flue gas system extensively. Noticing this gap in the literature, this study has introduced an empirical correlation model based on the Peng-Robinson equation of state (PR EoS), with fugacity expressions that are able to predict and describe the solid-fluid phase equilibria of the ternary system of the flue gas components (i.e. N₂-O₂-CO₂). The study covered wide ranges of pressure (from 5 to 130 bar) and temperature (140 to 220 K). Then, the model was optimized by applying it to selected pairs of the binary systems forming the flue gas with a possibility to form solid CO₂ (i.e., N₂-CO₂ and O₂-CO₂), where the optimum interaction parameters were determined to be 0.0405 and 0.1600, respectively. The model proved to be successful in generating and predicting the phase diagrams for these binary systems and for the ternary system (N₂-O₂-CO₂). Therefore, it was utilized to model and simulate a solid-vapor (SV) separation unit for CO₂ capture from flue gas mixtures.

Sensitivity analyses were conducted to evaluate the effects of the compressor discharge pressure and SV process temperature on various key parameters (namely, product gas composition and energy consumption) of the SV separation process. The SV unit was further compared to a traditional solvent-based CO₂ capture process that utilizes MDEA. Both processes were optimized to produce clean gas streams with CO₂ compositions of 0.3% or less. Simulation results proved that the SV separation unit achieves high removal

ratios of CO₂ and from the flue gas, while consuming less energy when compared to the industry-popular amine-based technology. Additionally, the SV process requires less process equipment than the amine-scrubbing process, hence requires a lower capital costs. Furthermore, and in the absence of the solvents and due to the low operating temperature, the equipment will not suffer from high corrosion rates; hence lower maintenance and operational costs are needed. It also results in less contaminated product gas streams.

The thermodynamic model proposed in this work provides a practical tool to study and predict the solid-fluid phase behavior of the ternary system (N₂-O₂-CO₂) at low temperatures, at which the solidification of CO₂ takes place. This model could be further developed to model and describe other SLVE of components found in flue gas streams, such as H₂S, CO, and NO_x gases. Expanding the model would allow to improve the capabilities of the corresponding SV separation unit. It is also recommended to build a lab-scale or pilot-scale of the SV unit to test its performance and compare to it to the simulation results, hence determining the efficiency of the process.

Author Contributions: H.A.: conceptualization, work execution, methodology, software, writing—original draft preparation. A.A.: work execution, software. S.A.A.-M.: conceptualization, methodology, supervision, validation, reviewing and editing. All authors have read and agreed to the published version of the manuscript.

Funding: This research received no external funding.

Data Availability Statement: All data generated or analyzed during this study are included in this article.

Acknowledgments: Open Access funding provided by the Qatar National Library.

Conflicts of Interest: The authors declare no conflict of interest.

References

1. Moazzem, S. *A Review on Technologies for Reducing CO₂ Emission from Coal Fired Power Plants*; Rasul, M.G., Ed.; IntechOpen: Rijeka, Croatia, 2012; p. 11.
2. Lettieri, P.; Yassin, L.; Simons, S.J.R. 7—Advanced thermal treatment of composite wastes for energy recovery. In *Woodhead Publishing Series in Composites Science and Engineering; Recycling and Reuse of Waste Composites*; Woodhead Publishing: Cambridge, UK, 2010; pp. 152–191. ISBN 978-1-84569-462-3.
3. Song, C.; Pan, W.; Srimat, S.T.; Zheng, J.; Li, Y.; Wang, Y.-H.; Xu, B.-Q.; Zhu, Q.-M. Tri-reforming of Methane over Ni Catalysts for CO₂ Conversion to Syngas With Desired H₂/CO Ratios Using Flue Gas of Power Plants Without CO₂ Separation. In *Carbon Dioxide Utilization for Global Sustainability*; Park, S.-E., Chang, J.-S., Lee, Eds.; Elsevier: Amsterdam, The Netherlands, 2004; Volume 153, pp. 315–322, ISBN 0167-2991.
4. Alalwan, H.A.; Alminshid, A.H. Science of the Total Environment CO₂ capturing methods: Chemical looping combustion (CLC) as a promising technique. *Sci. Total Environ.* **2021**, *788*, 147850. [[CrossRef](#)] [[PubMed](#)]
5. Kanniche, M.; Gros-Bonnivard, R.; Jaud, P.; Valle-Marcos, J.; Amann, J.-M.; Bouallou, C. Pre-combustion, post-combustion and oxy-combustion in thermal power plant for CO₂ capture. *Appl. Therm. Eng.* **2010**, *30*, 53–62. [[CrossRef](#)]
6. Godin, J.; Liu, W.; Ren, S.; Xu, C.C. Advances in recovery and utilization of carbon dioxide: A brief review. *J. Environ. Chem. Eng.* **2021**, *9*, 105644. [[CrossRef](#)]
7. Figueroa, J.D.; Fout, T.; Plasynski, S.I.; McIlvried, H.; Srivastava, R.D. Advances in CO₂ Capture Technology—The U.S. Department of Energy’s Carbon Sequestration Program. *Int. J. Greenh. Gas Control* **2008**, *2*, 9–20. [[CrossRef](#)]
8. Spigarelli, B.P.; Kawatra, S.K. Opportunities and challenges in carbon dioxide capture. *J. CO₂ Util.* **2013**, *1*, 69–87. [[CrossRef](#)]
9. Cuéllar-Franca, R.M.; Azapagic, A. Carbon capture, storage and utilisation technologies: A critical analysis and comparison of their life cycle environmental impacts. *J. CO₂ Util.* **2015**, *9*, 82–102. [[CrossRef](#)]
10. Wang, M.; Lawal, A.; Stephenson, P.; Sidders, J.; Ramshaw, C. Post-combustion CO₂ capture with chemical absorption: A state-of-the-art review. *Chem. Eng. Res. Des.* **2011**, *89*, 1609–1624. [[CrossRef](#)]
11. Shaw, R.; Mukherjee, S. The development of carbon capture and storage (CCS) in India: A critical review. *Carbon Capture Sci. Technol.* **2022**, *2*, 100036. [[CrossRef](#)]
12. Dunstan, M.T.; Donat, F.; Bork, A.H.; Grey, C.P.; Müller, C.R. CO₂ Capture at Medium to High Temperature Using Solid Oxide-Based Sorbents: Fundamental Aspects, Mechanistic Insights, and Recent Advances. *Chem. Rev.* **2021**, *121*, 12681–12745. [[CrossRef](#)]
13. Xu, Y.; Luo, C.; Sang, H.; Lu, B.; Wu, F.; Li, X.; Zhang, L. Structure and surface insight into a temperature-sensitive CaO-based CO₂ sorbent. *Chem. Eng. J.* **2022**, *435*, 134960. [[CrossRef](#)]

14. Qiao, Y.; Wu, C. Nitrogen enriched biochar used as CO₂ adsorbents: A brief review. *Carbon Capture Sci. Technol.* **2022**, *2*, 100018. [[CrossRef](#)]
15. Demir, H.; Aksu, G.O.; Gulbalkan, H.C.; Keskin, S. MOF Membranes for CO₂ Capture: Past, Present and Future. *Carbon Capture Sci. Technol.* **2022**, *2*, 100026. [[CrossRef](#)]
16. Kiani, S.; Taghizade, A.; Ramezani, R.; di Felice, R.; Molelekwa, G.F.; Mazinani, S. Enhancement of CO₂ removal by promoted MDEA solution in a hollow fiber membrane contactor: A numerical and experimental study. *Carbon Capture Sci. Technol.* **2022**, *2*, 100028. [[CrossRef](#)]
17. Ababneh, H.; Al-Muhtaseb, S. An Empirical Correlation-Based Model to Predict Solid-Fluid Phase Equilibria and Phase Separation of the Ternary System CH₄-CO₂-H₂S. *J. Nat. Gas Sci. Eng.* **2021**, *94*, 104120. [[CrossRef](#)]
18. Ababneh, H.; Al-muhtaseb, S.A. A Review on the Solid-Liquid-Vapor Phase Equilibria of Acid Gases in Methane. *Greenh. Gases Sci. Technol.* **2022**, *12*, 566–579. [[CrossRef](#)]
19. Font-Palma, C.; Cann, D.; Udemu, C. Review of Cryogenic Carbon Capture Innovations and Their Potential Applications. *J. Carbon Res.* **2021**, *7*, 58. [[CrossRef](#)]
20. Maqsood, K.; Mullick, A.; Ali, A.; Kargupta, K.; Ganguly, S. Cryogenic carbon dioxide separation from natural gas: A review based on conventional and novel emerging technologies. *Rev. Chem. Eng.* **2014**, *30*, 453–477. [[CrossRef](#)]
21. Valencia, J.A.; Denton, R.D.; Northrop, P.S.; Mart, C.J.; Smith, R.K. Controlled freeze zone technology for the commercialization of Australian high CO₂ natural gas. In *SPE Asia Pacific Oil & Gas Conference and Exhibition*; OnePetro: Adelaide, Australia, 2014; Volume 2, pp. 951–961. [[CrossRef](#)]
22. Sonntag, R.E.; Wylen, G.J. The Solid—Vapor Equilibrium of Carbon Dioxide—Nitrogen. *Adv. Cryog. Eng.* **1962**, *7*, 99–105. [[CrossRef](#)]
23. Smith, G.E.; Sonntag, R.E.; Wylen, G.J. Solid-Vapor Equilibrium of the Carbon Dioxide-Nitrogen System at Pressures to 200 Atmospheres. *Adv. Cryog. Eng.* **1964**, *9*, 197–206. [[CrossRef](#)]
24. Rest, A.J.; Scurlock, R.G.; Wu, M.F. The solubilities of nitrous oxide, carbon dioxide, Aliphatic ethers and alcohols, and water in cryogenic liquids. *Chem. Eng. J.* **1990**, *43*, 25–31. [[CrossRef](#)]
25. Yakimenko, N.P.; Gluch, G.M.; Iomtev, M.B.; Abramova, R.I. Solubility of Solid Carbon-Dioxide in Liquid-Nitrogen. *Zhurnal Fiz. Khimii* **1975**, *49*, 209–210.
26. Fedorova, M.F. The solubility of C₂H₂ and CO₂ in liquid nitrogen and oxygen. *Zhurnal Fiz. Khimii* **1940**, *14*, 422–426.
27. Schweitzer, O.R. *Solid-Liquid-Vapor Phase Equilibria in the Binary Systems: Ethylene—Carbon-Dioxide, Propane—Carbon-Dioxide, Nitrogen—Carbon-Dioxide, and Helium—Carbon-Dioxide*; Wayne State University: Detroit, MI, USA, 1962.
28. Fandiño, O.; Trusler, J.P.M.; Vega-Maza, D. Phase behavior of (CO₂+H₂) and (CO₂+N₂) at temperatures between (218.15 and 303.15)K at pressures up to 15MPa. *Int. J. Greenh. Gas Control* **2015**, *36*, 78–92. [[CrossRef](#)]
29. Amamchyan, R.G.; Bertsev, V.V.; Bulanin, M.O. Analysis of cryogenic solutions according to IR absorption spectra. *Zavod. Lab* **1973**, *39*, 432–434.
30. De Stefani, V.; Baba-Ahmed, A.; Valtz, A.; Meneses, D.; Richon, D. Solubility measurements for carbon dioxide and nitrous oxide in liquid oxygen at temperatures down to 90 K. *Fluid Phase Equilib.* **2002**, *200*, 19–30. [[CrossRef](#)]
31. De Guido, G.; Pellegrini, L.A. Calculation of solid-vapor equilibria for cryogenic carbon capture. *Comput. Chem. Eng.* **2022**, *156*, 107569. [[CrossRef](#)]
32. Peng, D.-Y.; Robinson, D.B. A New Two-Constant Equation of State. *Ind. Eng. Chem. Fundam.* **1976**, *15*, 59–64. [[CrossRef](#)]
33. Baxter, L.; Baxter, A.; Burt, S. Cryogenic CO₂ Capture as a Cost-Effective CO₂ Capture Process. In Proceedings of the 26th Annual International Pittsburgh Coal Conference 2009, Pittsburgh, PA, USA; 2009; Volume 1.
34. Maqsood, K.; Ali, A.; Nasir, R.; Abdulrahman, A.; Bin Mahfouz, A.; Ahmed, A.; Shariff, A.B.M.; Ganguly, S.; Mubashir, M.; Show, P.L. Experimental and simulation study on high-pressure V-L-S cryogenic hybrid network for CO₂ capture from highly sour natural gas. *Process Saf. Environ. Prot.* **2021**, *150*, 36–50. [[CrossRef](#)]
35. Tuinier, M.J.; van Sint Annaland, M.; Kuipers, J.A.M. A novel process for cryogenic CO₂ capture using dynamically operated packed beds—An experimental and numerical study. *Int. J. Greenh. Gas Control* **2011**, *5*, 694–701. [[CrossRef](#)]
36. Tuinier, M.J.; van Sint Annaland, M. Biogas Purification Using Cryogenic Packed-Bed Technology. *Ind. Eng. Chem. Res.* **2012**, *51*, 5552–5558. [[CrossRef](#)]
37. Seiler, M.; Groß, J.; Bungert, B.; Sadowski, G.; Arlt, W. Modeling of Solid/Fluid Phase Equilibria in Multicomponent Systems at High Pressure. *Chem. Eng. Technol.* **2001**, *24*, 607–612. [[CrossRef](#)]
38. Jäger, A.; Span, R. Equation of state for solid carbon dioxide based on the Gibbs free energy. *J. Chem. Eng. Data* **2012**, *57*, 590–597. [[CrossRef](#)]
39. Yokozeki, A. Analytical Equation of State for Solid-Liquid-Vapor Phases. *Int. J. Thermophys.* **2003**, *24*, 589–620. [[CrossRef](#)]
40. Ababneh, H.; Al-muhtaseb, S.A. Prediction of solid-liquid-vapor phase equilibria of noble gases in nitrogen. *Arab. J. Chem.* **2022**, *15*, 103866. [[CrossRef](#)]
41. Vera, J.H. Book Review: Molecular thermodynamics of fluid-phase equilibria by John M. Prausnitz, Rüdiger N. Lichtenthaler and Edmundo Comes de Azevedo, Third Edition, 1999. *Can. J. Chem. Eng.* **2000**, *78*, 429–430. [[CrossRef](#)]
42. Nikolaidis, I.K.; Boulougouris, G.C.; Peristeras, L.D.; Economou, I.G. Equation-of-State Modeling of Solid-Liquid-Gas Equilibrium of CO₂ Binary Mixtures. *Ind. Eng. Chem. Res.* **2016**, *55*, 6213–6226. [[CrossRef](#)]
43. Sandler, S.I. *Chemical, Biochemical, and Engineering Thermodynamics*; Wiley: Hoboken, NJ, USA, 2006.

44. Smith Van Ness, H.C.; Abbott Michael, M.J.M. *Introduction to Chemical Engineering Thermodynamics*; McGraw-Hill: Boston, MA, USA, 2005.
45. Ababneh, H.; AlNouss, A.; Karimi, I.A.; Al-Muhtaseb, S.A. Natural Gas Sweetening Using an Energy-Efficient, State-of-the-Art, Solid and Vapor Separation Process. *Energies* **2022**, *15*, 5286. [[CrossRef](#)]
46. Shakeel, H.; Wei, H.; Pomeroy, J.M. Measurements of enthalpy of sublimation of Ne, N₂, O₂, Ar, CO₂, Kr, Xe, and H₂O using a double paddle oscillator. *J. Chem. Thermodyn.* **2018**, *118*, 127–138. [[CrossRef](#)]
47. Aspen Technology, Inc. *Aspen Plus User Guide, Version 10.2, Aspen Plus®*; Aspen Technology, Inc.: Cambridge, MA, USA, 2000.
48. Riva, M. *Biomethane Purification Processes: Thermodynamic Study of Solid-Liquid-Vapor Equilibria of Methane-Rich Mixtures*; Université Paris Sciences et Lettres: Paris, France, 2016.
49. Rodriguez-Reartes, S.B.; Cismondi, M.; Zabaloy, M.S. Computation of solid-fluid-fluid equilibria for binary asymmetric mixtures in wide ranges of conditions. *J. Supercrit. Fluids* **2011**, *57*, 9–24. [[CrossRef](#)]
50. Riva, M.; Campestrini, M.; Toubassy, J.; Clodic, D.; Stringari, P. Solid-liquid-vapor equilibrium models for cryogenic biogas upgrading. *Ind. Eng. Chem. Res.* **2014**, *53*, 17506–17514. [[CrossRef](#)]
51. Jacobsen, R.T.; Stewart, R.B.; Jahangiri, M. Thermodynamic Properties of Nitrogen from the Freezing Line to 2000 K at Pressures to 1000 MPa. *J. Phys. Chem. Ref. Data* **1986**, *15*, 735–909. [[CrossRef](#)]
52. Von Henning, F.; Otto, J. Vapor-Pressure Curves and Triple Points in the Temperature Range from 14° to 90° Abs. *Phys. Z.* **1936**, *37*, 633.
53. Benamor, A.; Nasser, M.; Al-Marri, M.J. *Gas Processing Technology-Treatment and Utilization*; Abraham, M., Ed.; Elsevier: Oxford, UK, 2017; pp. 359–387. ISBN 978-0-12-804792-7.
54. Jenny Seagraves, R.H.; Weiland, I.O. Treating High CO₂ Gases with MDEA. 2009. Available online: <https://www.digitalrefining.com/article/1000573/treating-high-co2-gases-with-mdea#.Ysh8T3ZBw2x> (accessed on 25 August 2022).